JACS
JOURNAL OF THE AMERICAN CHEMICAL SOCIETY
Article
pubs.acs.org/JACS

The Big Impact of a Small Detail: Cobalt Nanocrystal Polymorphism as a Result of Precursor Addition Rate during Stock Solution Preparation

Nikos Liakakos,[†] Benoît Cormary,[†] Xiaojian Li,[†,‡] Pierre Lecante,[§] Marc Respaud,[†] Laurent Maron,[†] Andrea Falqui,[∥] Alessandro Genovese,[∥] Laure Vendier,[‡] Spyros Koïnis,[⊥] Bruno Chaudret,[†] and Katerina Soulantica*[,†]

[†]Université de Toulouse; INSA, UPS, CNRS, LPCNO, 135 avenue de Rangueil, 31077 Toulouse, France
[‡]Laboratoire de Chimie de Coordination (CNRS), BP 44099, 205 route de Narbonne, 31077 Toulouse, France
[§]Centre d'Elaboration de Matériaux et d'Etudes Structurales (CNRS), 29, rue Jeanne Marvig, 31055 Toulouse, France
[∥]Nanochemistry, Instituto Italiano di Tecnologia, Via Morego 30, 16163 Genova, Italy
[⊥]Department of Inorganic Chemistry, Faculty of Chemistry, University of Athens, Panepistimiopolis, 15771 Athens, Greece

Supporting Information

ABSTRACT: The control of nanocrystal structures at will is still a challenge, despite the recent progress of colloidal synthetic procedures. It is common knowledge that even small modifications of the reaction parameters during synthesis can alter the characteristics of the resulting nano-objects. In this work we report an unexpected factor which determines the structure of cobalt nanoparticles. Nanocrystals of distinctly different sizes and shapes have resulted from stock solutions containing exactly the same concentrations of $[Co\{N(SiMe_3)_2\}_2(thf)]$, hexadecylamine, and lauric acid. The reduction reaction itself has been performed under identical conditions. In an effort to explain these differences and to analyze the reaction components and any molecular intermediates, we have discovered that the rate at which the cobalt precursor is added to the ligand solution during the stock solution preparation at room temperature becomes determinant by triggering off a nonanticipated side reaction which consumes part of the lauric acid, the main stabilizing ligand, transforming it to a silyl ester. Thus, an innocent mixing, apparently not related to the main reaction which produces the nanoparticles, becomes the parameter which in fine defines nanocrystal characteristics. This side reaction affects in a similar way the morphology of iron nanoparticles prepared from an analogous iron precursor and the same long chain stabilizing ligands. Side reactions are potentially operational in a great number of systems yielding nanocrystals, despite the fact that they are very rarely mentioned in the literature.

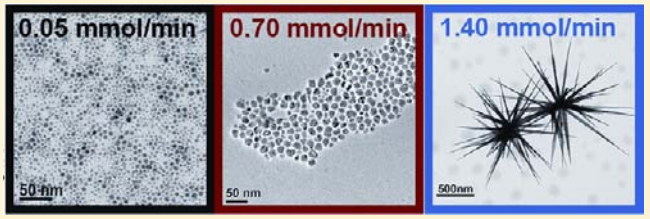

INTRODUCTION

Nanocrystals (NCs) are one of the cornerstones in the emergent era of nanosciences and nanotechnology. Numerous wet chemistry synthetic procedures developed during the last years have made available nanocrystals of various sizes, shapes, and compositions.[1] Syntheses by wet chemical routes involve in general rather complex reactions, which allow tailoring of NC characteristics and therefore their various properties. These procedures involve both molecular and solid-state reactions, while the transition of the matter from one state to the other is nearly impossible to follow by the characterization techniques available so far. In this respect, mechanistic approaches similar to those used in molecular chemistry are difficult to apply. However, many studies have succeeded in shedding some light on the mechanisms of nanocrystal formation, and several principles concerning NC shape control provide valuable information on general trends.[2] Even so, it is still unusual to obtain a specific NC morphology through the simple application of the general principles governing the NC formation. NC synthesis is still largely empirical, and while several aspects can be explained a posteriori, it is nearly impossible to predict the results of a reaction that involves new reactants. Specific unexpected aspects inherent to each reaction can turn out to be dominant over general principles.

In parallel, in order for NCs to be widely used in new applications for which they seem to be the candidates of choice, (i.e., optics, electronics, biology, medicine, and catalysis),[1] several issues have to be addressed. One of them, directly connected to their performance in any emerging application, is their reproducible synthesis. As for any chemical product, commercial NCs should be identical from one batch to another, since their properties directly depend on their size, size distribution, composition, shape, surface chemistry, etc. An irreproducible synthesis can therefore render useless a theoretically perfect candidate. Despite the technological

Received: May 9, 2012
Published: October 8, 2012

dx.doi.org/10.1021/ja304487b | J. Am. Chem. Soc. 2012, 134, 17922−17931

importance of reproducibility in NC synthesis, examples in the literature where this aspect is noted are extremely rare.[3]

This is especially true in complex solutions such as those using binary mixtures of organic surfactants, which have been successfully used for the preparation of size- and shape-controlled nanocrystals of various materials.[4] The selective reactivity of certain ligands toward different seed facets has been exploited in order to control the size and shapes of nanocrystals by kinetically controlling the growth rate of each facet. In addition to NC stabilization, ligands can also react in solution with molecular precursors to form new molecular species which, having different reactivities, will modify the nucleation and growth steps during nanocrystal synthesis.[5]

These ligand mixtures have been used in particular for the preparation of magnetic NCs, which are an example of technologically important materials, with applications spanning from biomedicine to ultrahigh-density magnetic recording and catalysis.[6] Their magnetic properties strongly depend upon their shape.[7] In this respect, cobalt nanomaterials have attracted considerable interest, due to their size- and shape-dependent magnetic properties which make them good candidates for several of the applications listed above.[8] The magnetic anisotropy of Co-NCs can be modulated by controlling their crystalline structure and shape. Several shapes of Co-NCs have been synthesized,[9] and the fact that cobalt can adopt different crystalline structures certainly accounts for the shape variety in which Co-NCs can grow.

Our group has been developing purely metallic magnetic nanoparticles of various shapes and sizes which are free from any native oxide layer.[9d,e,10] Among them, cobalt anisotropic nano-objects such as nanorods and nanowires are of special interest for applications in which magnetically hard materials are required. Monocrystalline cobalt nanorods spontaneously organized in superlattices have been initially obtained from our group, by reduction under H_2 of the organometallic precursor $[Co(\eta^3\text{-}C_8H_{13})(\eta^4\text{-}C_8H_{12})]$ in the presence of a long-chain amine and a long-chain acid.[9d,e] Later on, replacement of $[Co(\eta^3\text{-}C_8H_{13})(\eta^4\text{-}C_8H_{12})]$ by the silyl amide complex of cobalt $[Co\{N(SiMe_3)_2\}_2(thf)]$ gave rise to nanorods of improved size distribution and longer range organization.[11] Silyl amide complexes of cobalt and iron seem to be ideal precursors of nanoparticles, since they are easily reduced under hydrogen. For instance, the reduction of the silyl amide of iron $[Fe\{N(SiMe_3)_2\}_2]_2$ under H_2 in the presence of long-chain acid and long-chain amine ligands has given rise to iron and alloy nanocrystals of various sizes and shapes as well as to superlattices of nanocrystals.[10b−d]

Being particularly interested in cobalt nanocrystals and in order to achieve reproducible syntheses and optimize the results toward size and shape selectivity, we have undertaken a systematic study of the parameters affecting the reactions: reactant concentrations and ratios, temperature, pressure, etc. By a slight modification of the ratio between the ligands added, the morphology can be varied from spheres to nanorods and multipods, giving access to nanomaterials with different magnetic properties. The possibility of drastically changing the Co-NC morphology by minor variations of the reactant ratios and concentrations offers flexibility. It requires, however, very strict reaction procedures in order for the NCs to be reproducible from one synthesis to the other and complicates the rationalization of the role played by each reactant.

In this paper we report some unexpected results obtained with one system, $[Co\{N(SiMe_3)_2\}_2(thf)]$/LA/HDA (LA = lauric acid, HDA = hexadecylamine, thf = tetrahydrofuran), when the Co/LA/HDA ratio is 1/2.04/0.36. We came upon these findings when trying to understand the reasons this reaction kept giving irreproducible results, despite the fact that strictly identical conditions were applied during the reduction of the stock solution at 150 °C and under 3 bar of H_2. Indeed, the addition rate of the cobalt precursor to the LA/HDA mixture during the preparation of the stock solution at room temperature was the only parameter modified. Suprisingly, this addition rate alone is able to determine the morphology of Co-NCs. While only the specific ratio Co/LA/HDA = 1/2.04/0.36 is noted in the present work, it has to be mentioned that for high LA/HDA ratios a dependence of the final result on the addition rate has been observed. It has to be pointed out that in the present work no NCs are formed by the reactions taking place during stock solution preparation. It is only after heating this solution to 150 °C under H_2 that NCs are obtained. It has been reported previously that the injection rate of the precursor to the reaction mixture during the reaction plays a role in the shape of the chalcogenide, as well as metal and bimetallic NCs.[12] This injection rate defines the concentration of the precursor administration to the system during NC formation. It is therefore not unexpected to affect the kinetics of the NC nucleation and growth in a way analogous to a modification of the reaction temperature or reactant concentration. In the present case the addition rate does not concern directly the main reaction in which NCs are formed.

■ EXPERIMENTAL SECTION

Due to the air sensitivity of the metal precursors, as well as of the nanoparticles obtained, all experiments were performed under inert conditions, either by using Schlenk techniques or in the interior of a glovebox. Anhydrous anisole, packed and furnished under an inert atmosphere, was purchased from Aldrich (99.7%, anhydrous). It was transferred in the glovebox, and the traces of water were removed by activated molecular sieves. The cobalt precursor $[Co\{N(SiMe_3)_2\}_2(thf)]$ and the iron precursor $[Fe\{N(SiMe_3)_2\}_2]_2$ were purchased from NanoMeps. The LA was purchased from Acros (99%) and the HDA from Aldrich (98%), and they were used in the glovebox without any further purification. All glassware was carefully dried and introduced in the glovebox. The mixing of the reactants took place in the interior of the glovebox in a double-walled reaction vessel connected to a thermostated bath (Fisher Scientific, Polystat 37, stability 0.02 °C), kept at 25 °C. The stirring rate was always the same 750 rounds/min.

The procedure can be described by four steps.

Step I: Mixing of the Two Ligands HDA and LA. A 408 mg portion (2.04 mmol) of LA was dissolved in 10 mL of dry anisole. An 86.9 mg portion (0.36 mmol) of HDA was dissolved in 10 mL of dry anisole. These were transferred to a double-walled reactor in the interior of the glovebox, thermostated at 25 °C. The mixture was stirred for 3 min.

Step II: Addition of the $[Co\{N(SiMe_3)_2\}_2(thf)]$ to the Ligand Mixture. A solution of 452 mg (1 mmol) of $[Co\{N(SiMe_3)_2\}_2(thf)]$ in 2 mL of anisole was added to the ligand mixture. The addition rate was variable: **NC a**, 0.05 mmol/min; **NC b**, 0.70 mmol/min; **NC c**, 1.40 mmol/min. It has to be noted that these values are only indicative, since the $[Co\{N(SiMe_3)_2\}_2(thf)]$ solutions were manually added to the ligand mixture and a regular admission cannot be guaranteed. The best way to predict the tendency is by looking at the UV−vis spectrum. The final solutions were diluted to 24 mL ([Co] = 42 mM). An aliquot of the solution was transferred to a UV−vis cell. Another 10 mL aliquot of the solution was transferred to a Fischer−Porter vessel and subjected to hydrogen pressurization, while the rest of the solution was stirred at 25 °C in the glovebox for 5 days, during which time samples were taken in order to follow the evolution of the reaction in time.

dx.doi.org/10.1021/ja304487b | J. Am. Chem. Soc. 2012, 134, 17922−17931

Step III: Pressurisation under Hydrogen. The Fischer–Porter vessels were connected to a vacuum line while being stirred in a water bath at 25 °C. For each addition rate, 10 mL of the solution was subjected to pressurization with 3 bar of H_2 with stirring over 7 min, 25 min after the end of the $[Co\{N(SiMe_3)_2\}_2(thf)]$ addition to the ligand mixture. The rest of the solution was left to evolve at 25 °C in the glovebox for several days. A control reduction was performed at the end in order to see any modification of the nanocrystal morphology upon evolution of the solution.

Step IV: Nanoparticle Synthesis. The Fischer–Porter vessel was transferred to an oil bath preheated to 150 °C and left to react with stirring for 24 h. After the end of the reaction the Fischer–Porter vessels were transferred to the glovebox and TEM (transmission electron microscopy) samples were prepared by drop-casting the crude solution on a TEM grid.

The **NC a** solution was evaporated to dryness, since centrifugation did not result in precipitation of the nanoparticles. The SQUID (superconducting quantum interference device), WAXS (wide-angle X-ray scattering), XRD (X-ray diffraction), and EXAFS (extended X-ray absorption fine structure) experiments were performed on the resulting sticky solid. **NC b** and **NC c** were decanted and washed with toluene before SQUID, WAXS, XRD, and EXAFS characterization of the solid samples.

The same reactant concentrations and preparation procedures were used for the iron and cobalt nanoparticles.

For step I 170 mg (0.84 mmol) of LA was dissolved in 4 mL of dry anisole. A 36 mg portion (0.15 mmol) of HDA was dissolved in 4 mL of dry anisole. Then these solutions were transferred to a double-walled reactor in the interior of the glovebox, thermostated at 25 °C. The mixture was stirred for 3 min. For step II a solution of 158 mg (0.21 mmol) of $[Fe\{N(SiMe_3)_2\}_2]_2$ in 2 mL of dry anisole was added to the ligand mixture. Steps III and IV were performed exactly as in the case of cobalt.

Two different addition rates have been employed: slow addition, 0.05 mmol/min; fast addition, 1.40 mmol/min.

Preparation of $[Co(LA)_2]$. A solution of lauric acid (1.58 g, 7.9 mmol in 25 mL toluene) was rapidly added to a solution of $[Co\{N(SiMe_3)_2\}_2(thf)]$ (1.53 g, 3.39 mmol in 5 mL of toluene) in a Schlenk tube under argon with vigorous stirring. The green color of the $[Co\{N(SiMe_3)_2\}_2(thf)]$ solution turned to blue-violet upon addition. The system was stirred for 48 h. The blue solid that formed was filtered under argon, washed two times with pentane, and dried under vacuum.

Anal. Found (calcd): C, 62.94 (62.95); H, 9.99 (10.05). IR: $\nu_{as}(COO^-)$ 1522 cm^{-1}, $\nu_{sym}(COO^-)$ 1457 cm^{-1}.[13] UV–vis: λ_1 589 nm (ε_1 = 365 L $mol^{-1}cm^{-1}$), λ_2 =539 nm (ε_1 = 234 L $mol^{-1}cm^{-1}$) (see Figure S1 in the Supporting Information).

Conventional TEM imaging was performed using a JEOL JEM 1011 microscope, equipped with a W thermionic electron source and a Mega-View Olympus CCD camera and working at an acceleration voltage of 100 kV, or with a JEOL JEM 1400 microscope equipped with LaB_6 thermionic electron source and working at an acceleration voltage of 120 kV. The high-resolution TEM (HREM) analysis has been carried out using JEOL JEM 2100F and JEOL JEM 2200FS microscopes, both equipped with a field emission gun (FEG) and a Gatan Ultrascan 1000 CCD camera and working at an acceleration voltage of 200 kV. The microscope JEM 2200FS was also equipped with a CEOS spherical aberration corrector of the objective lens. The structural features of the nanostructures imaged by HREM were studied by means of 2D Fourier analysis.

XRD data were obtained on a Panalytical Empyrean instrument with samples enclosed by two Kapton foils in order to avoid sample oxidation during measurement. Source Co: Kα1= 1.789 010 Å. For the calculation of the crystallite size in **NC b**, the Scherrer equation was used. In this case the crystallite size was found to be about 5 nm, much smaller than the size seen by TEM. Instrumental broadening of diffraction peaks was calibrated with highly crystalline silicon powder as an external reference. **NC a** did not give an exploitable diffraction pattern.

WAXS measurements were performed at CEMES-CNRS. Samples were sealed in 1 mm diameter Lindemann glass capillaries. Data collection was performed using a dedicated two-axis diffractometer with graphite-monochromated Mo Kα radiation (λ = 0.7107 Å). A typical measurement time was 15 h. The PDFs (pair distribution functions) were obtained after Fourier transformation of the reduced intensity functions.

EXAFS measurements at the Co K absorption edge were performed at HASYLAB in Hamburg on beamline C in transmission mode at room temperature. Data analysis was performed using the Athena software.

Magnetization measurements were performed using MPMS SQUID with superconductor interference detectors. Dried powders of the samples were sealed in gelatin capsules in a glovebox under an Ar atmosphere to prevent any oxidation. Only the raw data are shown in the Supporting Information. Note that the whole diamagnetic contribution (gelatin capsule and molecular compounds) is less than 0.1% of the magnetism due to the Co nanoparticles.

The UV–vis spectra were recorded on a Perkin-Elmer Lambda 35 spectrometer. Aliquots of the solutions 25 min after $[Co\{N(SiMe_3)_2\}_2(thf)]$ addition to the ligand mixture were transferred to a 2 mm optical path UV cell. The spectra were recorded with a sampling scan rate of 240 nm/min and a resolution of 1 nm.

The ^1H NMR spectra were obtained from toluene-d_8 solutions on a Bruker Avance 500 spectrometer.

Single-crystal X-ray data were collected at low temperature (180 K) on an Xcalibur Oxford Diffraction diffractometer using graphite-monochromated Mo Kα radiation (λ = 0.710 73 Å) and equipped with an Oxford Instrument Cooler Device. The final unit cell parameters were obtained by means of a least-squares refinement. The structures were solved by direct methods using SIR92[14] and refined by means of least-squares procedures on F^2 with the aid of the program SHELXL97[15] including the software package WinGX version 1.63.[16] The atomic scattering factors were taken from ref 17. All hydrogen atoms were geometrically placed and refined by using a riding model. All non-hydrogen atoms were anisotropically refined, and in the last cycles of refinement a weighting scheme was used, where weights were calculated from the formula $w = 1/[\sigma^2(F_o^2) + (aP)^2 + bP]$, with $P = (F_o^2 + 2F_c^2)/3$. The drawing of the molecule was performed with the program ORTEP32[18] with 30% probability displacement ellipsoids for non-hydrogen atoms.

Computational details for the theoretical calculations are given in the Supporting Information.

RESULTS AND DISCUSSION

In Figure 1 we present TEM micrographs and the corresponding WAXS spectra from three different samples prepared by mixing at 25 °C $[Co\{N(SiMe_3)_2\}_2(thf)]$ (**1**) with LA and HDA in a 1/2.04/0.36 molar ratio and by the subsequent heating of the resulting solution for 24 h at 150 °C under 3 bar of H_2. All solutions had exactly the same concentration and were submitted to identical treatments during the reduction. Therefore, at first sight nothing could explain the dramatic size and structural differences observed between the resulting nanocrystals. The precise synthetic procedure as detailed in the Experimental Section consists of four steps. The first step is the mixing of LA and HDA solutions in anisole. During the second step a solution of **1** in anisole is added to the LA-HDA mixture. The third step is the pressurization of the solution with H_2, which acts as a reducing agent. The fourth and last step is the heating of the mixture. The NCs are produced only during the last step. By careful examination of the procedure, we discovered that the apparently small detail that made the difference was the rate of cobalt precursor addition to the LA/HDA mixture during the preparation of the starting solution in the second step.

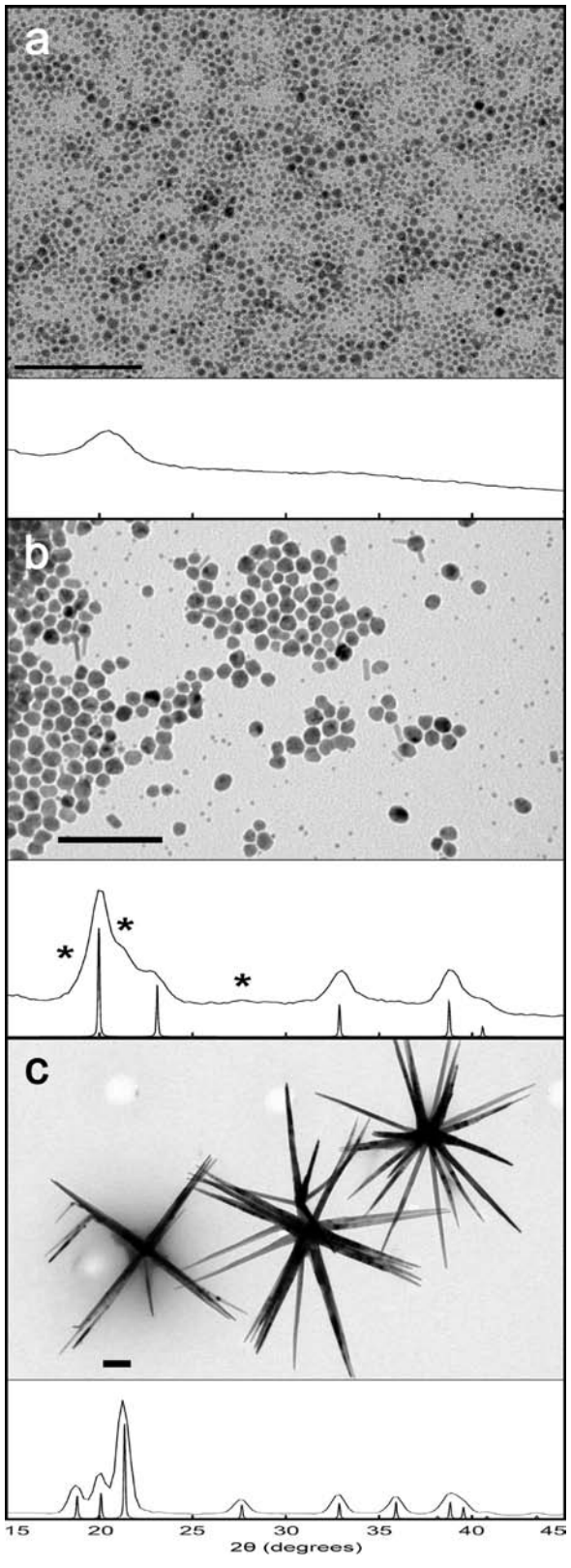

Figure 1. TEM micrographs and corresponding WAXS spectra of nano-objects obtained by different $[Co\{N(SiMe_3)_2\}_2(thf)]$ addition rates to the LA/HDA mixture: (a) slow addition; (b) intermediate addition; (c) fast addition (TEM scale bars 100 nm).

The nanoparticles of Figure 1a (**NC a**) were prepared by a *slow addition* of **1** to the ligand mixture (0.05 mmol/min) and display a mean diameter of 4.6 nm (σ = 0.9 nm), while those of Figure 1b (**NC b**) were prepared by an *intermediate addition* rate (0.70 mmol/min) and have a mean diameter of 13.7 nm (σ = 2 nm). The multipods in Figure 1c (**NC c**) were prepared by the *fast addition* of **1** to the ligand mixture (1.40 mmol/min). Their size is not very homogeneous, but they are much larger than **NC a** and **NC b** (general view in Figure S2 (Supporting Information)).

WAXS analyses in the reciprocal space clearly show that **NC b** and **NC c** are well crystallized, pure metallic cobalt NCs. The major peaks in each case match those of bulk metal in the face-centered cubic (*fcc*) and hexagonal close packed (*hcp*) structures, respectively, with identical cell parameters. In addition, minor features observed for **NC b** (marked with stars) point to the presence of a small quantity of material displaying the *hcp* structure. The analysis for **NC a** is more ambiguous: only broad peaks can be observed. This is not caused by the smaller particle size. In fact, the coherence length observed on the WAXS PDF (see Figure S3 in the Supporting Information) is close to 2.5 nm, significantly smaller than the size observed by TEM but large enough to produce detailed patterns for well-ordered metallic particles. Their pattern in real space is, however, poorly resolved and does not allow a clear indexation of the structure. Complementary EXAFS measurements have also been performed (see Figure S4 in the Supporting Information). They clearly confirm the metallic character of cobalt in all samples and evidence a well-defined local order. They are quite similar for all three colloids (besides size and/or static disorder effects on amplitude).

XRD measurements on several samples resulting from intermediate addition rates show that an increase of the addition rate increases the *hcp* component (see Figure S5 in the Supporting Information). Nevertheless, the presence of small quantities of the *fcc* phase in **NC c** cannot be discarded.

Careful analysis of the HREM (see Figure S6 in the Supporting Information) revealed the presence of both *hcp* and *fcc* phases for **NC a** and **b**. It has not been possible to analyze the **NC c** central core by HREM due to the thickness of the objects in this area, while their arms adopt a *hcp* crystalline structure.

Finally, the magnetization measurements were performed by SQUID for all samples **NCs a**–**NC c. NC b** and **NC c** display saturation magnetization (M_s) values consistent with purely metallic Co nanoparticles (see Figure S7 in the Supporting Information).

Thus, WAXS, XRD, EXAFS, SQUID, and HREM data point toward well-crystallized metallic objects for **NC b** and **NC c** and for **NC a** toward a material at a very early stage of crystallization mostly composed of small particles with a strong chemical order but still lacking the long-range order required to generate sharp patterns by X-ray diffraction.

All these techniques allow the characterization of the NCs and confirm their morphological and structural differences but do not allow us to understand the reason different addition rates result in such different NCs. The results obtained indicate that a *slow addition*, which gives rise to **NC a**, favors an extended nucleation, giving rise to small particles, while a *fast addition*, which gives rise to **NC c**, results in a limited nucleation, thus forming larger objects.[3a] Since the NC characteristics are determined before any reduction by H_2 takes place, it is in the initial solution composition that the reasons for these differences should be investigated.

While monitoring the reactions by NMR is not possible, due to the presence of paramagnetic and ferromagnetic species,

dx.doi.org/10.1021/ja304487b | J. Am. Chem. Soc. 2012, 134, 17922–17931

electronic spectroscopy can give information about the solution composition before reaction with H_2. In Figure 2 we present

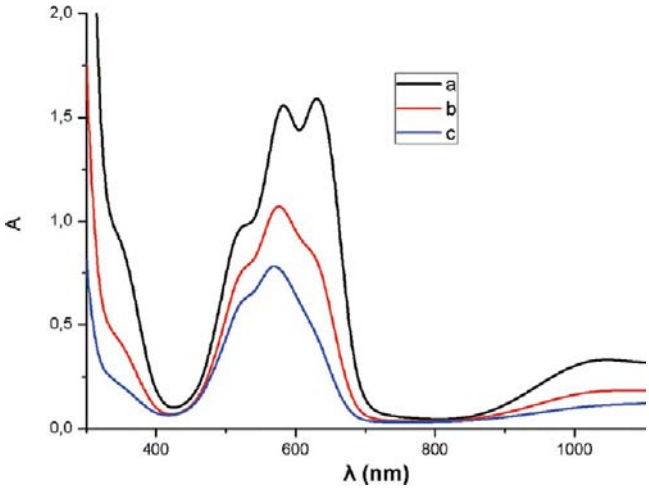

Figure 2. UV−vis spectra of the starting solutions obtained after the various cobalt addition rates 25 min after Co addition ([Co] = 42 mM, optical path 2 mm): (a) slow addition giving rise to **NC a**; (b) intermediate addition giving rise to **NC b**; (c) fast addition giving rise to **NC c**.

the electronic spectra of the stock solutions giving rise to **NC a**−**NC c**, recorded 25 min after addition of **1** to the ligand mixture and before pressurization with H_2 (see the Experimental Section). The spectrum of the precursor **1** has a characteristic peak at 680 nm (Figure S8 in the Supporting Information). This peak is absent in all **NC a**−**NC c** stock solutions, indicating that **1** is rapidly transformed into new species after its addition to the ligand mixture. Another observation is that all spectra consist of three strongly overlapping bands at ca. 630, 580, and 520 nm. However, some differences among the three solutions are obvious. For instance, the relative intensity of the peak at 630 nm decreases as the addition rate increases, becoming barely visible in the **NC c** starting solution. Taking into account the size of the resulting NCs, we could attribute this peak to some easily reducible Co species which under H_2 provides numerous primary nuclei and may be considered as a nucleation "reservoir". Additional spectra of intermediate rate additions and the corresponding NCs are presented in Figure S9 (Supporting Information), which shows a good qualitative correlation between the spectra and the NC characteristics. Thus, the UV−vis spectra reveal the presence of several cobalt species in solution before H_2 admission, the ratio and nature of which surprisingly depend on the cobalt addition rate.

Considering the sensitivity of the results to the stock solution composition and the dependence of this composition on such a small detail as the mixing rate, an interesting question that arises is for how long the stock solutions can be kept without affecting the reproducibility of the results. If reduction is performed when the stock solution is not yet in equilibrium, and if upon equilibration the nature of the species is modified with respect to the initial situation, this could affect the final resullts. As previously mentioned, for both *fast* and *slow addition*, **1** is rapidly consumed just after its addition to the LA/HDA mixture. This event was followed by slower evolutions which were monitored over time and are shown in Figure 3. In the absence of a thermostated spectrometer and in order to

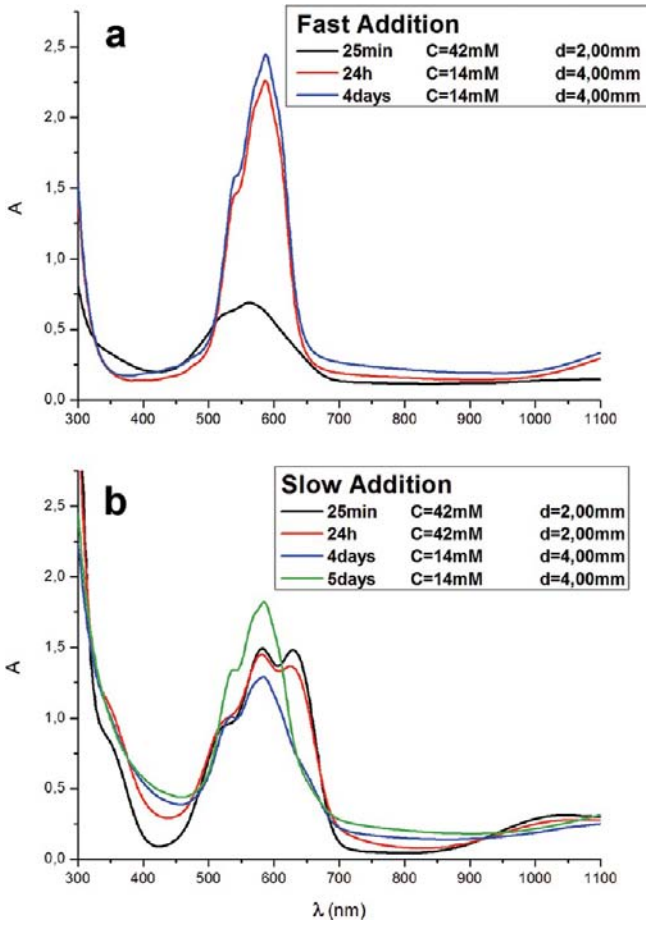

Figure 3. The evolution in time of *fast* and *slow addition* solutions: (black spectra) 25 min; (red spectra) 24 h; (blue spectra) 4 days. For the *slow addition* the green spectrum was taken at 5 days. Note that the high molecular absorbance of $[Co(LA)_2]$ has imposed an important dilution of the samples at longer reaction times.

follow the evolution of the solution which was stirred at 25 °C in the glovebox, aliquots of this solution were measured after 25 min, 24 h, and 4 days and, for the *slow addition* reaction, once more at 5 days. While soon after mixing, the UV−vis spectra are quite different for different addition rates (Figure 2), they are much less so after longer reaction times, where the main compound appears to be the same for both *fast* and *slow addition* solutions (compare for instance the blue lines of parts a and b of Figure 3). We can also notice an important evolution of both spectra with time, which however is not accompanied by an important modification of the NC characteristics. Thus, reduction under H_2 at 150 °C of a solution aged for some days produces nanocrystals similar to those resulting from a fresh solution, in the case of both a **slow** and a **fast** addition. These observations question the validity of the correlation between the solution spectra and the NC morphology and require further investigation.

In an effort to identify the species formed during the procedures of *slow addition* and *fast addition* and to understand better the reaction pathway, several UV−vis control experiments were performed. Interestingly, the spectrum of the *fast addition* after 24 h is almost identical with that of independently synthesized $[Co(LA)_2]$ (**2**), (Figure S1b in the Supporting Information). This is the main evolution in time observable for the *fast addition* solution. A very similar evolution has been

dx.doi.org/10.1021/ja304487b | J. Am. Chem. Soc. 2012, 134, 17922−17931

detected during the independent synthesis of $[Co(LA)_2]$ from **1** and LA (see Figure S10 in the Supporting Information). It is therefore likely that this evolution corresponds to the slow transformation of $[Co(LA)_2(thf)]$ (**3**) to $[Co(LA)_2]$.

Since the reduction of a freshly prepared *fast addition* solution in which $[Co(LA)_2(thf)]$ has not yet been transformed to $[Co(LA)_2]$ and of an "aged" *fast addition* solution in which $[Co(LA)_2(thf)]$ has been converted to $[Co(LA)_2]$ give essentially the same kind of multipods, albeit slightly smaller, we assume that these two compounds behave similarly toward reduction with H_2: that is, they are reduced slowly and constitute the growth reservoir.

For the *slow addition*, the transformation of $[Co(LA)_2(thf)]$ to $[Co(LA)_2]$ is also observable by UV−vis but is slower and yields less $[Co(LA)_2]$. In addition to this evolution, the intensity of the peak at 630 nm, attributed to the unidentified easily reducible Co species, decreases, with a simultaneous increase of the absorption in the UV region (Figure 3b). Since in this case also reduction under H_2 at 150 °C gives very similar results, either with a freshly prepared stock solution or with a solution which was left to evolve over some days, we believe that even if the intensity of the peaks attributed to an easily reducible compound are reduced with time, this nucleation "reservoir" does not evolve toward stable compounds but rather forms easily reducible species such as clusters. This evolution could correspond to the appearance of the intense absorption in the UV.

Theoretical calculations regarding the stability of several mononuclear analogues likely to exist in solution (see Figure S11 in the Supporting Information) are not incompatible with this transformation, since despite its slightly lower stability, $[Co(LA)_2]$ is much less soluble than $[Co(LA)_2(thf)]$. These calculations also indicate that HDA-containing species such as $[Co(LA)_2(HDA)(thf)]$ (**4**), $[Co(LA)_2(HDA)]$ (**5**), and $[Co(LA)_2(HDA)_2]$ (**6**) should also be present in the medium (Table 1). They are not detectable by UV−vis, but this is expected, considering the low amount of HDA present in solution.

Table 1. Main Species Potentially Present in the Reaction Mixtures, Their Corresponding Numbering, and Their Calculated Analogues

species[a]	calcd analogues[b]	energy[c]
$[Co\{N(SiMe_3)_2\}_2(thf)]$ (**1**)	$[Co\{N(SiMe_3)_2\}_2(thf)]$	+6.2
$[Co(LA)_2]$ (**2**)	$[Co(OOCPr)_2]$	−50.0
$[Co(LA)_2(thf)]$ (**3**)	$[Co(OOCPr)_2(thf)]$	−53.4
$[Co(LA)_2(HDA)(thf)]$ (**4**)	$[Co(OOCPr)_2(H_2NMe)(thf)]$	−57.3
$[Co(LA)_2(HDA)]$ (**5**)	$[Co(OOCPr)_2(H_2NMe)]$	−62.0
$[Co(LA)_2(HDA)_2]$ (**6**)	$[Co(OOCPr)_2(H_2NMe)_2]$	−68.8

[a]Species in solution; numbering as in the text. [b]Calculated analogues. [c]Energy in kcal/mol with respect to $[Co\{N(SiMe_3)_2\}_2]$.

The HDA-containing species may participate in both nucleation and growth steps. Indeed, while $[Co(LA)_2]$ alone cannot be reduced to nanoparticles under the conditions employed in this work, the addition of 2 equiv of HDA to a solution of $[Co(LA)_2]$ allows the formation of cobalt multipods with very long "pods", as shown in Figure 4. This result can be explained by a limited and slow nucleation giving rise to a small number of seeds on which Co overgrowth takes place. It is possible that the reaction with hydrogen is facilitated if an amine proton is present. Heterolytic activation of dihydrogen could then occur through coordination to Lewis acidic complexes and deprotonation by an amine; this is a well-documented process in coordination chemistry.[19]

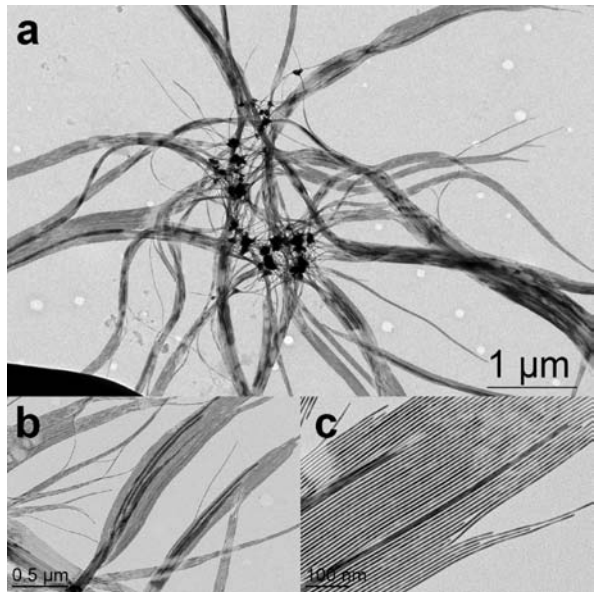

Figure 4. Cobalt multipods with very long "pods" obtained after heating at 150 °C under 3 bar of H_2 during 24 h a solution of $[Co(LA)_2]$, containing 2 equiv of HDA: (a) overview; (b and c) higher magnifications of the "pods".

Considering the results presented hereabove, we suggest that the *fast addition* solution is composed of small quantities of HDA-containing species (**4**−**6**), small quantities of the unknown nucleation "reservoir", and high quantities of $[Co(LA)_2(thf)]$ or $[Co(LA)_2]$ (depending on its aging time), which constitute the main growth "reservoir".

Even if the above experiments have given some information concerning the nature of the growth "reservoir", they do not explain the reason the rate of addition of **1** to the ligand mixture predetermines the increased proportion of this "reservoir" in the *fast addition* stock solution.

Since electronic spectroscopy does not provide direct structural information concerning the species formed in solution, several efforts have been dedicated to the isolation of complexes present in solution, in order to characterize them independently and confirm their presence in the stock solutions by UV−vis detection. Various ligand ratios have been used. While mixtures have been obtained in all cases, when we reacted 1 equiv of precursor **1** with a mixture of 3 equiv of LA and 1 equiv of HDA in anisole and heated the mixture to 60 °C for one night, a crimson gel was formed upon cooling, from which a few pink crystals were recovered. We have been able to determine their structure by single-crystal X-ray studies, and we were surprised to find out that the amine coordinated to the Co center was neither the HDA nor $HN(SiMe_3)_2$, which could have been liberated after LA deprotonation and coordination, but NH_3. The molecular structure of this compound, $[Co(LA)_2(NH_3)_2]$, is presented in Figure 5. Its energy with respect to $[Co\{N(SiMe_3)_2\}_2]$ is calculated to be −69.5 kcal/mol. Details on the structure and the packing of the molecules are given in Figure S12 (Supporting Information).

This structure indicates that the initially present $HN(SiMe_3)_2$ can be transformed in a relatively easy way. NH_3 could be logically produced only by the reaction of $HN(SiMe_3)_2$ with 2

dx.doi.org/10.1021/ja304487b | J. Am. Chem. Soc. 2012, 134, 17922−17931

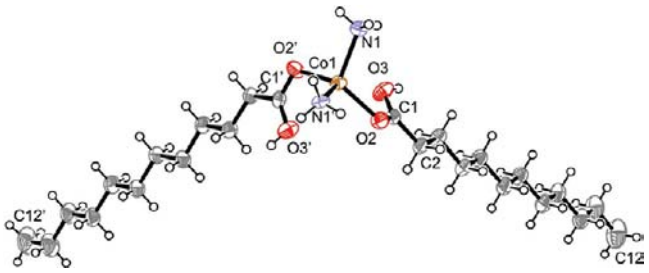

Figure 5. ORTEP view of the complex $[Co(LA)_2(NH_3)_2]$ (molecular formula $C_{24}H_{52}CoN_2O_4$) with ellipsoids drawn at the 30% probability level and with partial atom numbering for clarity. The molecule crystallizes in the monoclinic system (space group $C1_2/c1$).

equiv of LA, which is present in excess with respect to Co, with the concomitant formation of a silyl ester. While not useful for the identification of the species by UV−vis, this finding gave an important indication which prompted us to focus our attention on the possibility of this side reaction being operational even at room temperature: i.e., during the preparation of the stock solutions. In order to verify this possibility, the ^{1}H NMR spectra of the two extreme cases (*fast addition* and *slow addition* solutions) in toluene-d_8 were recorded. In contrast to the peaks of the coordinated ligands, which experience the effects of the presence of paramagnetic metal centers, the peaks of the free ligands in solution are not shifted with respect to their normal values. In Figure 6 we present the ^{1}H NMR spectra of the *fast addition* and *slow addition* solutions in toluene-d_8, 30 min after the addition of **1** to the ligand mixture.

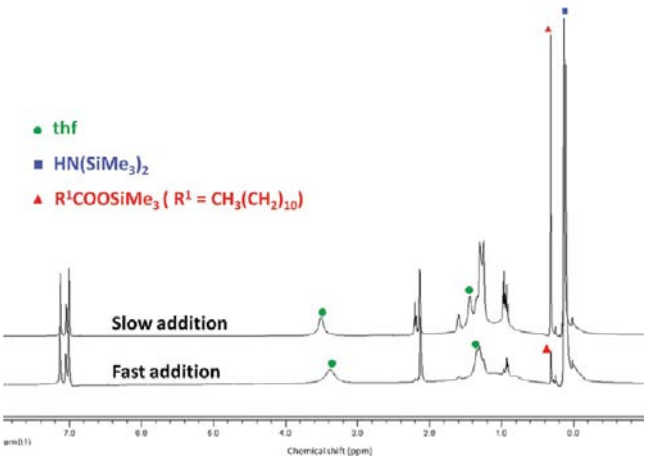

Figure 6. ^{1}H NMR spectra of solutions in toluene-d_8. The signals marked with a green circle belong to thf, the blue squares mark the methyl groups of free $HN(SiMe_3)_2$, and the red triangles indicate the methyl groups attached to Si in $R^1COOSiMe_3$ ($R^1 = CH_3(CH_2)_{10}$).

They both show the presence of free $HN(SiMe_3)_2$, the methyl protons of which appear at 0.12 ppm. However, the most interesting information, which is the key point of the differences observed between **NC a** and **NC c**, is given by the existence of a peak at 0.31 ppm corresponding to the methyl protons of the silyl ester $R^1COOSiMe_3$ ($R^1 = CH_3(CH_2)_{10}$), as confirmed by control experiments (see Figure S13 in the Supporting Information) and from literature data.[20] This is the product of the parallel reaction of LA with $HN(SiMe_3)_2$, which is liberated from **1**. The spectra confirm that this reaction is operational even at room temperature and, more importantly, indicate that only very little silyl ester is produced during the *fast addition* procedure, while the *slow addition* solution contains a significantly higher amount of this compound. The reason for the difference observed between the two solutions is that, during a *slow addition*, the first quantities of **1** come in contact with an excess of LA. Part of the LA reacts with **1**, hence liberating $HN(SiMe_3)_2$. This amine can react further with two molecules of LA, eventually producing two silyl ester molecules. The quantity of acid available for coordination to cobalt is therefore depleted and becomes less than 2 equiv. Carboxylates are known to stabilize Co in its molecular form.[21] Thus, in addition to small amounts of the bis-carboxylate complexes, cobalt amide species are present in large quantities and allow an easy nucleation step which can lead, according to their concentration, to small- or medium-sized nanoparticles. This side reaction is much less pronounced in the *fast addition* procedure because of the preference for LA to coordinate to Co and produce a bis(carboxylate) complex rather than react with $HN(SiMe_3)_2$.

To summarize, in the *fast addition* stock solution, most LA is coordinated to Co, either as $[Co(LA)_2(thf)]$ or as $[Co(LA)_2]$, which are stable and constitute the growth "reservoir". There are very few primary nuclei, resulting from less stable nonidentified species and/or the amine assisted decomposition of the bis(laurate) complexes. The reversible attachment of amines allows the coalescence of the primary nuclei into polycrystalline particles displaying *fcc* or *hcp* domains, which correspond to the cores of the multipods. The **NC c** shape, with clearly distinct domains, points toward a modification of the growth mechanism at a certain point of the reaction. Thus, after core formation and as the reaction proceeds, the consumption of the growth "reservoir" starts to liberate lauric acid. Upon liberation, its consumption by free $HN(SiMe_3)_2$ is in competition with its interaction with the NC surface. Nevertheless, when its concentration becomes significant enough to allow interaction with the cores, it will coordinate on the growing nanoparticles.[21,22] This interaction is facet selective and lets the (111) facets of *fcc* or (002) facets of *hcp* structured domains of the core be exposed to the incoming cobalt atoms. The "pods" may hence grow, incorporating Co atoms on the free (002) *hcp* or (111) *fcc* facets. The laurate ligand which continues to be liberated is coordinated along the *c* axis of the *hcp* structure in which the pods grow. Any transition from an *fcc* to *hcp* structure during this growth can be explained by the easy creation of stacking faults along the *c* axis. This proposed mechanism for the *fast addition* solution is outlined in Scheme 1.

In the case of *slow addition*, nucleation is easier and a large part of the cobalt is consumed in an extended nucleation step. The remaining growth "reservoir" is much less abundant, and therefore the liberated LA is less available for NC stabilization. The isotropic shape of **NC a** is probably also due to its low crystallinity, as evidenced by WAXS, which prevents the formation of well-defined facets that laurate could selectively stabilize.

Hence for both *fast* and *slow addition* solutions, the compositions are qualitatively the same but the proportion between the nucleation and growth reservoirs is very different. This difference accounts for the observed diversity of NC characteristics obtained in this work.

The knowledge acquired from this study has solved the problem of an irreproducible synthesis and has helped to identify compounds likely to constitute the nucleation and

Scheme 1. Proposed Reaction Pathway for the *Fast Addition* Stock Solution

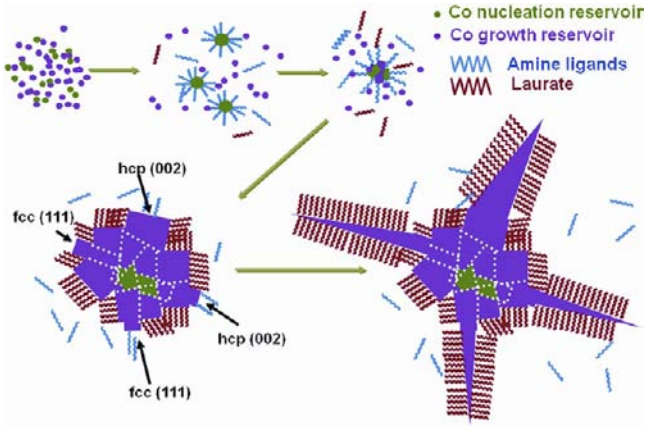

growth reservoirs. A well-controlled preparation of the stock solution, i.e. control of the addition rate, temperature, and stirring rate, will always yield the same product, when followed by the same reduction procedure. This means that an automatic pump delivery system has to be used, in order to guarantee not only the addition rate but also a regular flow during this addition. It is important to note that while what we have learned is not sufficient for tailoring the nanocrystal characteristics at will, it is indispensable for any further study aiming at fine-tuning the NC characteristics. We have to point out that there are better ways than controlling the mixing rate in order to modulate the size and shape of the nanocrystals, such as modifying the reduction reaction parameters as well as the Co/LA/HDA ratio, provided that a fast addition guarantees the coordination of the LA to the Co without ester formation. It is obvious that, without taking into account the side reaction between $HN(SiMe_3)_2$ and LA, any systematic variation of reaction parameters such as concentration and ratio of reactants, temperature, pressure, etc. can only give misleading information and provoke misinterpetations of the experimental results observed.

In order to find out whether or not this reaction is specific to cobalt, we tested the same approach with a similar precursor of iron, $[Fe\{N(SiMe_3)_2\}_2]_2$, an iron source used previously by our group for the synthesis of iron nano-objects.[10d,23] In Figure 7 we present the nanocrystals obtained under the same reaction conditions as in the case of cobalt. The same tendency is observed for this case also; however, apart from the presence of spherical NC in the *slow addition*, the shape remains roughly cubic for both cases since, under the conditions employed in the present work, Fe can only adopt a *bcc* (body-centered cubic) structure. The nanocrystals obtained by a *slow addition* of $[Fe\{N(SiMe_3)_2\}_2]_2$ to the LA/HDA mixture have a mean size of about 10 nm, while those produced by a *fast addition* are much larger with a mean size of about 130 nm. This reaction may therefore be expected in all cases where a silyl amide ligand and a long-chain acid are present in the system.

The importance of this work does not reside in the originality of the NCs presented. It is also well documented in the literature that solutions containing different concentrations of precursors of distinct stabilities yield different NCs, which is in fact the ultimate consequence of the silyl ester formation. What is interesting is the unexpected way by which the concentrations of the various precursors are modulated by a hidden parameter and the danger of misinterpretation of the

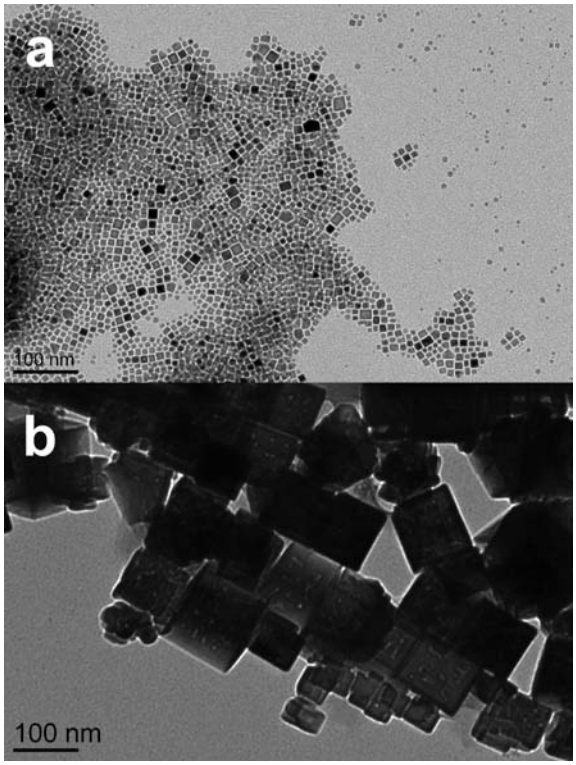

Figure 7. Iron nanocrystals obtained with a Fe/LA/HDA ratio of 1/2/0.36 in anisole at 150 °C after 24 h reaction by (a) *slow* and (b) *fast addition* of the precursor to the ligand mixture (scale bars 100 nm).

results if this parameter is ignored. The discovery of the role the side reaction played in the present work has not been straightforward, because the irreproducible results were initially attributed to some parameter of the reduction reaction and not to the preparation of the stock solution.

■ CONCLUSIONS

This work has shown how apparently insignificant details may have dramatic effects on the final result of a nanoparticle synthetic procedure.[24] Unless information to the contrary is confirmed, any stage of a reaction can be determinant for its final outcome, even the stages that are a priori beyond any suspicion. This example also illustrates the importance of rigorous synthetic protocols or, even better, automated procedures in order to have reproducible, operator-independent syntheses in complex reaction systems such as the majority of those employed in solution-grown NCs. The analysis of the present case also shows the importance of molecular chemistry in nanocrystal synthesis. The ligands cannot be considered only as stabilizers and regulators of the growth rate of the various crystallographic facets. Apart from this role, which is undeniably very important, they modify the nature and the relative concentrations of the species which compose the NC "reservoir" in solution, and this effect keeps on operating for the duration of the decomposition reaction. Eventually, the organic molecules present in solution can themselves be modified, raising some questions about the real nature of the surfactants which stabilize the NC surface, especially after being submitted to high temperatures. Even if this side reaction seems to be specific to a limited number of precursors, that is, those containing a silylamide as a ligand, it is likely that parasite reactions are operational in various other systems. This could,

dx.doi.org/10.1021/ja304487b | J. Am. Chem. Soc. 2012, 134, 17922−17931

for instance, be the case for the hot injection method, for which heating a mixture of organic reactants often close to their decomposition temperature prior to precursor injection is a common practice. Side reactions such as irreversible ester formation between stearic acid and 1-octadecanol in the presence of ZnO NCs[3b] and history-dependent reactivity of the precursors has been mentioned before,[25] but for the large majority of the reports where this aspect can play a role, this role is either not considered or not noted.

■ ASSOCIATED CONTENT

Supporting Information

Figures, tables, and a CIF file giving TEM and HREM complementary micrographs, XRD spectra of various addition rates, WAXS and EXAFS data and SQUID measurements for **NC a**−**NC c**, UV−vis spectra for various addition rates of the precursor $[Co\{N(SiMe_3)_2\}_2(thf)]$ and of control experiments, X-ray structure details and molecule packing in the crystal, NMR spectra of independent formation of the ester $CH_3(CH_2)_{10}COOSiMe_3$, computational details, and crystallographic data. This material is available free of charge via the Internet at http://pubs.acs.org.

■ AUTHOR INFORMATION

Corresponding Author

*E-mail: ksoulant@insa-toulouse.fr.

Notes

The authors declare no competing financial interest.

■ ACKNOWLEDGMENTS

We thank the ANR for the projects BATMAG and CARMA, the Région Midi-Pyrénées, the European Commission for the POCTEFA Interreg project (MET-NANO EFA 17/08), and the European Commission for the ERC AdG 246763 project for financial support. We thank A. Mari for SQUID measurements, TEMSCAN service for the microscopy, and C. Bijani for the NMR spectra.

■ REFERENCES

(1) (a) Manna, L.; Scher, E. C.; Alivisatos, A. P. *J. Am. Chem. Soc.* **2000**, *122*, 12700. (b) Hu, J.; Li, L.-S.; Yang, W.; Manna, L.; Wang, L.-W.; Alivisatos, A. P. *Science* **2001**, *292*, 2060. (c) Murray, R. W. *Chem. Rev.* **2008**, *108*, 2688. (d) Hyeon, T. *Chem. Commun.* **2003**, 927. (e) Tao, A. R.; Habas, S.; Yang, P. *Small* **2008**, *4*, 310. Kwon, S. G.; Hyeon, T. *Acc. Chem. Res.* **2008**, *41*, 1696. (f) Talapin, D. V.; Lee, J.-S.; Kovalenko, M. V.; Shevchenko, E. V. *Chem. Rev.* **2010**, *110*, 389. (g) Sau, T. K.; Rogach, A. L. *Adv. Mater.* **2010**, *22*, 1781. (h) Wang, X.; Zhuang, J.; Peng, Q.; Li, Y. *Nature* **2005**, *437*, 121.

(2) (a) Yin, Y.; Alivisatos, A. P. *Nature* **2005**, *437*, 664. (b) Xia, Y.; Xiong, Y.; Lim, B.; Skrabalak, S. E. *Angew. Chem., Int. Ed.* **2009**, *48*, 60. (c) Finney, E. E.; Finke, R. G. *J. Colloid Interface Sci.* **2008**, *317*, 351. (d) Zhang, J.; Huang, F.; Lin, Z. *Nanoscale* **2010**, *2*, 18. (e) Kumar, S.; Nann, T. *Small* **2006**, *2*, 316. (f) Kwon, S. G.; Hyeon, T. *Small* **2011**, *7*, 2685.

(3) (a) Shevchenko, E. V.; Talapin, D. V.; Schnablegger, H.; Kornowski, A.; Festin, O.; Svedlindh, P.; Haase, M.; Weller, H. *J. Am. Chem. Soc.* **2003**, *125*, 9090. (b) Chen, Y.; Kim, M.; Lian, G.; Johnson, M. B.; Peng, X. *J. Am. Chem. Soc.* **2005**, *127*, 13331.

(4) (a) Peng, X.; Manna, L.; Yang, W.; Wickham, J.; Scher, E.; Kadavanich, A.; Alivisatos, A. P. *Nature* **2000**, *404*, 59. (b) Seo, J.; Jun, Y.; Ko, S. J.; Cheon. *J. Phys. Chem. B* **2005**, *109*, 5389. (c) Zeng, H.; Rice, P. M.; Wang, S. X.; Sun, S. *J. Am. Chem. Soc.* **2004**, *126*, 11458.

(5) (a) Peng, Z. A.; Peng, X. *J. Am. Chem. Soc.* **2001**, *123*, 1389. (b) Xie, R.; Li, Z.; Peng, X. *J. Am. Chem. Soc.* **2009**, *131*, 15457. (c) Rempel, J. Y.; Bawendi, M. G.; Jensen, K. F. *J. Am. Chem. Soc.* **2009**, *131*, 4479. (d) Bao, Y.; An, W.; Turner, C. H.; Krishnan, K. M. *Langmuir* **2010**, *26*, 478. (e) Owen, J. S.; Chan, E. M.; Liu, H.; Alivisatos, A. P. *J. Am. Chem. Soc.* **2010**, *132*, 18206.

(6) (a) Sun, S.; Murray, C. B.; Weller, D.; Folks, L.; Moser, A. *Science* **2000**, *287*, 1989. (b) Zeng, H.; Li, J.; Liu, J. P.; Wang, Z. L.; Sun, S. *Nature* **2002**, *420*, 395. (c) Lu, A.-H.; Salabas, E. L.; Schüth, F. *Angew. Chem., Int. Ed.* **2007**, *46*, 1222. (d) Frey, N. A.; Peng, S.; Cheng, K.; Sun, S. *Chem. Soc. Rev.* **2009**, *38*, 2532. (e) Behrens, S. *Nanoscale* **2011**, *3*, 877. (f) Scariot, M.; Silva, D. O.; Scholten, J. D.; Machado, G.; Teixeira, S. R.; Novak, M. A.; Ebeling, G.; Dupont, J. *Angew. Chem., Int. Ed.* **2008**, *47*, 9075. (g) Dai, Q.; Nelson, A. *Chem. Soc. Rev.* **2010**, *39*, 4057. (h) Jang, Y.; Kim., S.; Jun, S. W.; Kim, B. H.; Hwang, S.; Song, I. K.; Kim, B. M.; Hyeon, T. *Chem. Commun.* **2011**, *47*, 3601.

(7) (a) Sorescu, M.; Brand, R. A.; Mihaila-Tarabanasu, D.; Diamandescu, L. *J. Appl. Phys.* **1999**, *85*, 5546. (b) Sellmyer, D. J.; Zheng, M.; Skomski, R. *J. Phys.: Condens. Matter.* **2001**, *13*, R433. (c) Binns, C.; Maher, M. J.; Pankhurst, Q. A.; Kechrakos, D.; Trohidou, K. N. *Phys. Rev. B* **2002**, *66*, 184413.

(8) (a) Puntes, V. F.; Krishnan, K. M.; Alivisatos, A. P. *Appl. Phys. Lett.* **2001**, *78*, 2187. (b) Soulantica, K.; Wetz, F.; Maynadié, J.; Falqui, A.; Tan, R. P.; Blon, T.; Chaudret, B.; Resoaud, M. *Appl. Phys. Lett.* **2009**, *95*, 152504. (c) Schrittwieser, S.; Ludwig, F.; Dieckhoff, J.; Soulantica, K.; Viau, G.; Lacroix, L.-M.; Lentijo Mozo, S.; Boubekri, R.; Maynadié, J.; Huetten, A.; Brueckl, H.; Schotter, J. *ACS Nano* **2012**, *6*, 791. (d) Zhang, Q.; Kang, J.; Wang, Y. *ChemCatChem* **2010**, *2*, 1030. (e) O'Handley, R. C. *Modern Magnetic Materials: Principles and Applications*; Wiley: New York, 1999.

(9) (a) Dinega, D. P.; Bawendi, M. G. *Angew. Chem., Int. Ed.* **1999**, *38*, 1788. (b) Sun, S.; Murray, C. B. *J. Appl. Phys.* **1999**, *85*, 4325. (c) Puntes, V. F.; Zanchet, D.; Erdonmez, C. K.; Alivisatos, A. P. *J. Am. Chem. Soc.* **2002**, *124*, 12874. (d) Dumestre, F.; Chaudret, B.; Amiens, C.; Respaud, M.; Fejes, P.; Renaud, P.; Zurcher, P. *Angew. Chem., Int. Ed.* **2003**, *42*, 5213. (e) Dumestre, F.; Chaudret, B.; Amiens, C.; Fromen, M.-C.; Casanove, M.-J.; Renaud, P.; Zurcher, P. *Angew. Chem., Int. Ed.* **2002**, *41*, 4286. (f) Ciuculescu, D.; Dumestre, F.; Comesana-Hermo, M.; Chaudret, B.; Spasova, M.; Farle, M.; Amiens, C. *Chem. Mater.* **2009**, *21*, 3987. (g) Soumare, Y.; Garcia, C.; Maurer, T.; Chaboussant, G.; Ott, F.; Fiévet, F.; Piquemal, J.-Y.; Viau, G. *Adv. Funct. Mater.* **2009**, *19*, 1971.

(10) (a) Cordente, N.; Respaud, M.; Senocq, F.; Casanove, M.-J.; Amiens, C.; Chaudret, B. *Nano Lett.* **2001**, *1*, 565. (b) Dumestre, F.; Chaudret, B.; Amiens, C.; Renaud, P.; Fejes, P. *Science* **2004**, *303*, 821. (c) Desvaux, C.; Amiens, C.; Fejes, P.; Renaud, P.; Respaud, M.; Lecante, P.; Snoeck, E.; Chaudret, B. *Nat. Mater.* **2005**, *4*, 750. (d) Lacroix, L.-M.; Lachaize, S.; Falqui, A.; Respaud, M.; Chaudret, B. *J. Am. Chem. Soc.* **2009**, *131*, 549.

(11) Wetz, F.; Soulantica, K.; Respaud, M.; Falqui, A.; Chaudret, B. *Mater. Sci. Eng., C* **2007**, *27*, 1162.

(12) (a) Cozzoli, P. D.; Manna, L.; Curri, M. L.; Kudera, S.; Giannini, C.; Striccoli, M.; Agostiano, A. *Chem. Mater.* **2005**, *17*, 1296. (b) Shieh, F.; Saunders, A. E.; Korgel, B. A. *J. Phys. Chem. B* **2005**, *109*, 8538. (c) Nair, P. S.; Fritz, K. P.; Scholes, G. D. *Chem. Commun.* **2004**, *18*, 2084. (d) Zhang, H.; Li, W.; Jin, M.; Yu, T.; Yang, D.; Xia, Y. *Nano Lett.* **2011**, *11*, 898. (e) Zeng, J.; Zhu, C.; Tao, J.; Jin, M.; Zhang, H.; Li, Z.-Y.; Zhu, Y.; Xia, Y. *Angew. Chem., Int. Ed.* **2012**, *51*, 2354.

(13) Nakamoto, K. *Infrared and Raman Spectra of Inorganic and Coordination Compounds*, 6th ed.; Wiley: Hoboken, NJ, 2009.

(14) Altomare, A.; Cascarano, G.; Giacovazzo, C.; Guagliardi, A. *J. Appl. Crystallogr.* **1993**, *26*, 343.

(15) Sheldrick, G. M. *Programs for Crystal Structure Analysis (Release 97-2)*; Institüt für Anorganische Chemie der Universität, Tammanstrasse 4, D-3400 Göttingen, Germany, 1998.

(16) Farrugia, L. *J. Appl. Crystallogr.* **1999**, *32*, 837.

(17) *International Tables for X-Ray Crystallography*; Kynoch Press: Birmingham, England, 1974; Vol. *IV*.

(18) Farrugia, L. J. *J. Appl. Crystallogr.* **1997**, *30*, 565.

(19) Dobereiner, G. E.; Nova, A.; Schley, N. D.; Hazari, N.; Miller, S. J.; Eisenstein, O.; Crabtree, R. H. *J. Am. Chem. Soc.* **2011**, *133*, 7547.

(20) Kabalka, G. W.; Bierer, D. E. *Organometallics* **1989**, *8*, 655.

(21) (a) Samia, A. C. S.; Hyzer, K.; Schlueter, J. A; Qin, C.-J.; Jiang, J. S.; Bader, S. D.; Lin, X.-M. *J. Am. Chem. Soc.* **2005**, *127*, 4126. (b) Samia, A. C. S.; Schlueter, J. A.; Jiang, J. S.; Bader, S. D.; Qin, C.-J.; Lin, X.-M. *Chem. Mater.* **2006**, *18*, 5203.
(22) (a) Liu, H.; Guo, J.; Yin, Y.; Augustsson, A.; Dong, C.; Nordgren, J.; Chang, C.; Alivisatos, P.; Thornton, G.; Ogletree, D. F.; Requejo, F. G.; de Groot, F.; Salmeron, M. *Nano Lett.* **2007**, *7*, 1919. (b) Shevchenko, E. V.; Talapin, D. V.; Rogach, A. L.; Kornowski, A.; Haase, M.; Weller, H. *J. Am. Chem. Soc.* **2002**, *124*, 11480. (c) Wu, N.; Fu, L.; Su, M.; Aslam, M.; Wong, K. C.; Dravid, V. P. *Nano Lett.* **2004**, *4*, 383.
(23) Lacroix, L.-M.; Lachaize, S.; Hüe, F.; Gatel, C.; Blon, T.; Tan, R. P.; Carrey, J.; Warot-Fonrose, B.; Chaudret, B. *Nano Lett.* **2012**, *12*, 3245.
(24) (a) Lim, S. I.; Ojea-Jimenez, I.; Varon, M.; Casals, E.; Arbiol, J.; Puntes, V. *Nano Lett.* **2010**, *10*, 964. (b) Ojea-Jimenez, I.; Bastus, N. G.; Puntes, V. *J. Phys. Chem. C* **2011**, *115*, 15752.
(25) (a) Peng, Z. A.; Peng, X. *J. Am. Chem. Soc.* **2002**, *124*, 3343. (b) Xiong, Y.; Washio, I.; Chen, J.; Sadilek, M.; Xia, Y. *Angew. Chem., Int. Ed.* **2007**, *46*, 4917.